Thermonuclear reaction rate of $^{17}O(p,\gamma)^{18}F$

C. Fox, C. Iliadis, A. E. Champagne, R. P. Fitzgerald, R. Longland, J. Newton, J. Pollanen, and R. Runkle
Department of Physics and Astronomy, University of North Carolina, Chapel Hill, North Carolina, 27599-3255, USA, and Triangle Universities Nuclear Laboratory, Durham, North Carolina 27708-0308, USA
(Received 26 January 2005; published 5 May 2005)

The $^{17}O(p,\gamma)^{18}F$ and $^{17}O(p,\alpha)^{14}N$ reactions have a profound influence on hydrogen-burning nucleosynthesis in a number of stellar sites, including red giants, asymptotic giant branch (AGB) stars, massive stars, and classical novae. Previously evaluated thermonuclear rates for both reactions carry large uncertainties. We investigated the proton-capture reaction on ^{17}O in the bombarding energy range of $E_p^{lab} = 180$–540 keV. We observed a previously undiscovered resonance at $E_R^{lab} = 193.2 \pm 0.9$ keV. The resonance strength amounts to $(\omega\gamma)_{p\gamma} = (1.2 \pm 0.2) \times 10^{-6}$ eV. With this value, the uncertainties of the $^{17}O(p,\gamma)^{18}F$ reaction rates are reduced by orders of magnitude in the peak temperature range of classical novae ($T = 0.1$–0.4 GK). We also report on a reevaluation of the $^{17}O(p,\gamma)^{18}F$ reaction rates at lower temperatures that are pertinent to red giants, AGB stars, or massive stars. The present work establishes the $^{17}O(p,\gamma)^{18}F$ reaction rates over a temperature range of $T = 0.01$–1.5 GK with statistical uncertainties of 10–50%. The new recommended reaction rates deviate from the previously accepted values by an order of magnitude around $T \approx 0.2$ GK and by factors of 2–3 at $T < 0.1$ GK.

DOI: 10.1103/PhysRevC.71.055801 PACS number(s): 26.30.+k, 24.30.Gd, 25.40.Lw, 26.50.+x

I. INTRODUCTION

The $^{17}O(p,\gamma)^{18}F$ and $^{17}O(p,\alpha)^{14}N$ reactions are parts of the carbon-nitrogen-oxygen (CNO) cycles. Precise knowledge of their thermonuclear reaction rates is of paramount importance for understanding hydrogen-burning nucleosynthesis in a number of different stellar sites. The stellar temperature ranges of primary interest amount to $T = 0.03-0.1$ GK, e.g., for red giants, asymptotic giant branch (AGB) stars, or massive stars, and to $T = 0.1-0.4$ GK, e.g., for classical novae. According to the Nuclear Astrophysics Compilation of Reaction Rates (NACRE) [1], the thermonuclear rates for both of these reactions carry large uncertainties. Results for the $^{17}O(p,\gamma)^{18}F$ reaction are shown in Fig. 1. For a better comparison, we show the reaction rate ratio of the previously accepted upper (or lower) limit and the recommended rate. It can be seen that the reaction rates at temperatures important for classical novae are uncertain by several orders of magnitude. It was demonstrated recently [2] that such large errors introduce significant variations in C, N, O, and F isotopic abundances that are predicted by hydrodynamical nova simulations. These variations, in turn, have far-reaching implications for the galactic synthesis of ^{17}O, the stellar production of the radioisotope ^{18}F, and the predicted oxygen isotopic ratios in nova ejecta [2].

The errors shown in Fig. 1 are mainly caused by an unmeasured narrow resonance. An energy level diagram of ^{18}F is displayed in Fig. 2. The resonance corresponds to a previously observed state at $E_x = 5786$ keV ($J^\pi = 2^-$) [3] in the ^{18}F compound nucleus. The γ-ray decay of this state is also known. Transitions to the levels at $E_x = 937$ and $E_x = 1081$ keV have been reported, with branching ratios of 40 and 60%, respectively [3]. The expected location of the resonance is $E_R^{lab} \approx 190$ keV, as calculated from the excitation energy and the Q value for the $^{17}O(p,\gamma)^{18}F$ reaction ($Q_{p\gamma} = 5606.5 \pm 0.5$ keV [4]). We report here on the measurement of this previously unmeasured resonance in the $^{17}O(p,\gamma)^{18}F$ reaction. As will be seen, our new results reduce the uncertainties of the $^{17}O(p,\gamma)^{18}F$ reaction rates by orders of magnitude in the peak temperature range of classical novae ($T = 0.1$–0.4 GK). A preliminary account of the present work has been given elsewhere, and all of our present results supersede those published earlier [2]. We also report on a reevaluation of the $^{17}O(p,\gamma)^{18}F$ reaction rates at lower temperatures that are of interest to red giants or AGB stars. At these lower temperatures, our new reaction rates differ by factors of 2–3 from those presented by the NACRE Collaboration [1].

The present work is organized as follows. Section II describes the experimental equipment used in our measurements. In Sec. III, we discuss experimental procedures and results. Thermonuclear reaction rates for the $^{17}O(p,\gamma)^{18}F$ reaction are presented in Sec. IV. Conclusions are given in Sec. V. Throughout this work, E_p and E_R denote the proton bombarding energy and the resonance energy, respectively. All quantities are given in the laboratory system unless mentioned otherwise.

II. EXPERIMENTAL EQUIPMENT

The experiment was carried out at the Laboratory for Experimental Nuclear Astrophysics (LENA), located at the Triangle Universities Nuclear Laboratory (TUNL). A 1 MV JN Van de Graaff accelerator supplied proton beams of up to 100 μA on target in the energy range of $E_p = 140$–540 keV. The bombarding energy was calibrated with the well-known $^{18}O(p,\gamma)^{19}F$ resonance at $E_R = 150.82 \pm 0.09$ keV [5]. The uncertainty in absolute energy and the energy spread were ± 1 and 2.5 keV, respectively. The proton beam entered the target chamber through a liquid-nitrogen-cooled copper tube that was biased to -300 V in order to suppress the emission of secondary electrons from the target and the beam collimator. The target and chamber formed a Faraday cup for charge integration. The beam was focused into a profile of ≈ 6 mm

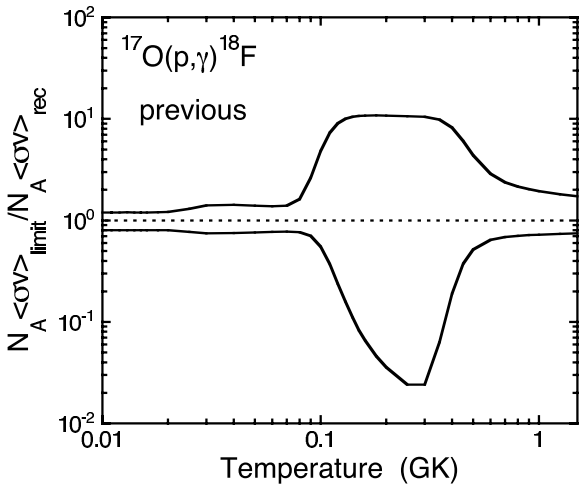

FIG. 1. Reaction rates for the ^{17}O$(p,\gamma)^{18}$F reaction [1] prior to the present work. The solid lines show the ratios of the upper (or lower) reaction rate limit to the recommended rates. The area between the solid lines represents the previous uncertainty in the reaction rate ratio.

diameter on target. The target was directly water cooled using deionized water.

Targets were prepared by anodization of 0.5 mm thick tantalum backings in ^{17}O- or ^{18}O-enriched water. According to the supplier, the enrichments amounted to 90.0 and 97.3%, respectively. Note, that different targets (with an ^{17}O enrichment of 83.8%) were used in our preliminary study [2]. Such targets have been found [6] to be of well-defined stoichiometry (Ta_2O_5) with a target thickness that is precisely determined by the anodizing voltage. Prior to target preparation, the surface of the tantalum backing was etched [7] in order to remove some of the impurities that are a source of beam-induced background radiation. All targets were checked frequently, and no degradation in yield or target thickness was observed during the course of the experiment.

Prompt γ rays from the ^{17}O$(p,\gamma)^{18}$F and ^{18}O$(p,\gamma)^{19}$F reactions were detected using a large-volume (582 cm^3) HPGe detector placed at an angle of 0° and a distance of 16 mm from the target. Accurate energy calibrations were obtained from radioactive sources, background contributions (^{40}K and ^{208}Tl), and well-known decays in the ^{14}N$(p,\gamma)^{15}$O reaction. The energy resolution was typically 2.5 keV at $E_\gamma = 1.33$ MeV. Peak efficiency calibrations were established using ^{152}Eu and ^{56}Co sources and the decays from well-known resonances in the ^{14}N$(p,\gamma)^{15}$O, ^{26}Mg$(p,\gamma)^{27}$Al, and ^{27}Al$(p,\gamma)^{28}$Si reactions. The full-energy peak efficiency amounted to ≈5% at a γ-ray energy of 1.33 MeV. Since the γ-ray detector was placed in very close geometry to the target, coincident summing corrections [8] had to be considered carefully in all of our measured spectra. The corrections were performed numerically according to the matrix formalism described by Ref. [9]. The required total efficiency values were measured using ^{54}Mn, ^{137}Cs, and ^{60}Co sources. The total efficiency calibration was extended to a γ-ray energy of 12 MeV by performing Monte Carlo calculations using the code MCNP. The experimental setup, including detector housing,

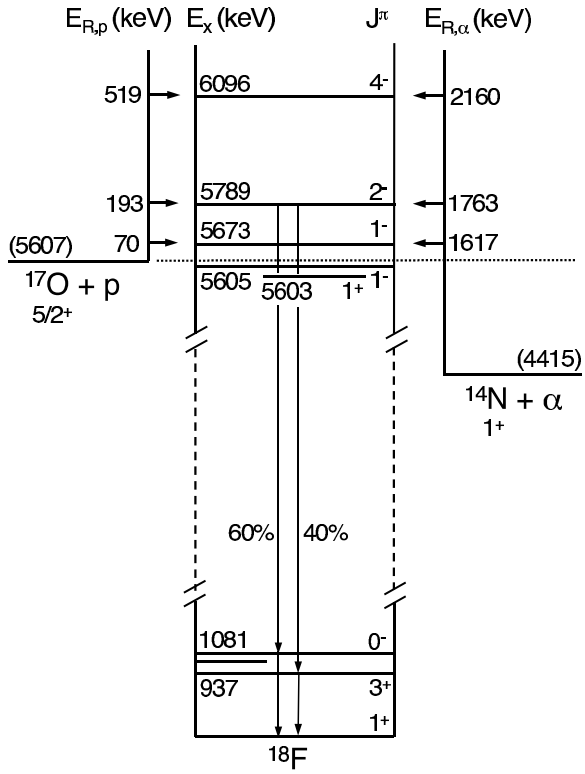

FIG. 2. Relevant parts of the energy level diagram for the ^{18}F compound nucleus. Most energies and J^π values are from Refs. [3,4]. Those for the second excited state above the proton threshold are from the present work (see Table I). The values in parenthesis represent proton and α-particle separation energies. Resonance energies are given in the laboratory system.

contact rod, mounts, shielding, target holder, and chamber, was included in the simulations. The solid angle attenuation coefficients needed for angular correlation corrections were also estimated using MCNP.

III. EXPERIMENTAL PROCEDURES AND RESULTS

A sample excitation function (i.e., γ-ray yield versus bombarding energy) of a previously observed resonance in the ^{17}O$(p,\gamma)^{18}$F reaction is shown in Fig. 3. The target thickness amounts to about 9 keV at $E_p \approx 0.52$ MeV, as can be seen from the full width at half maximum of the excitation function. The resonance energy is obtained from the location of the midpoint of the low-energy edge of the excitation function. The result is $E_R = 518.9 \pm 1.0$ keV. Our value agrees with the literature value of $E_R = 518.9 \pm 1.3$ keV that is obtained from the excitation energy for the corresponding ^{18}F level ($E_x = 6096.4 \pm 1.1$ keV [3]) and the reaction Q value. The resonance strength is defined by

$$(\omega\gamma)_{xy} = \frac{(2J+1)}{(2j_t+1)(2j_p+1)}\frac{\Gamma_x\Gamma_y}{\Gamma}, \qquad (1)$$

with J, j_t, and j_p the spin of the resonance, target, and projectile, respectively; Γ_x, Γ_y, and Γ denote the partial widths of the incoming and outgoing reaction channel and the total width of the resonance. The resonance strength is

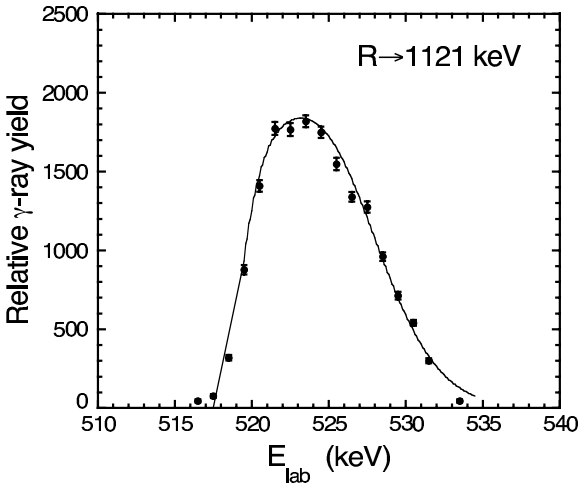

FIG. 3. Excitation function of the primary $R \rightarrow 1121$ keV transition for the previously observed $^{17}O(p,\gamma)^{18}F$ resonance at $E_R = 519$ keV. A total of six excitation functions have been measured for this resonance during the course of the experiment. All were consistent in yield height and target thickness. The solid line represents a numerical simulation showing the expected thick-target yield when the beam energy resolution and energy straggling in the target are taken into account.

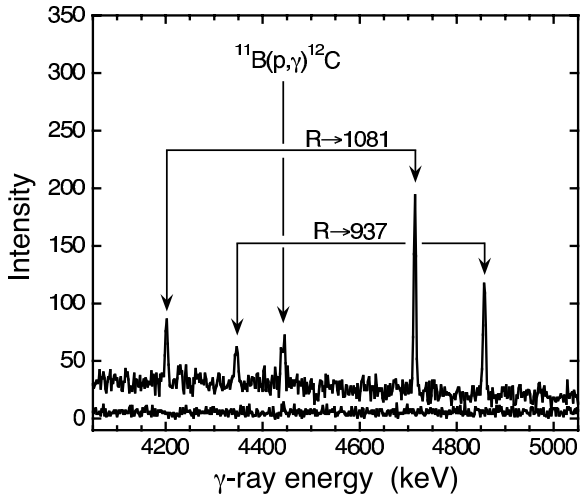

FIG. 4. Relevant sections of on-resonance (upper) and off-resonance (lower) γ-ray spectra measured at $E_p = 200$ and 228 keV, respectively. The two primary γ-ray decays of the previously unmeasured $E_R = 193$ keV resonance to the ^{18}F levels at 937 and 1081 keV are clearly observed in the on-resonance spectrum. Shown are the full-energy and single-escape peaks for each of the primary transitions. The peak at $E_\gamma \approx 4440$ keV is caused by a ^{11}B contamination in the target.

experimentally obtained from the expression [10]

$$\omega\gamma = \frac{2}{\lambda^2}\epsilon_{\text{eff}}\frac{N_\gamma}{N_p}, \tag{2}$$

with λ the de Broglie wavelength, N_p the number of incident protons as calculated from the collected charge, and N_γ the resonant γ-ray intensity that is measured on the plateau of the thick-target yield curve. The quantity N_γ was corrected for peak efficiencies and coincident summing. Angular correlation effects were estimated but found to be negligible for this resonance considering the large solid angle covered by our detector. The effective stopping power for our oxygen targets is given by Bragg's rule

$$\epsilon_{\text{eff}} = \epsilon(^{17}\text{O}) + \frac{N(^{16}\text{O})}{N(^{17}\text{O})}\epsilon(^{16}\text{O}) + \frac{N(\text{Ta})}{N(^{17}\text{O})}\epsilon(\text{Ta}), \tag{3}$$

where N_i denotes the number densities of atoms. Stopping powers ϵ_i are obtained from the code SRIM [11]. All quantities in Eq. (2) are given in the center-of-mass system. Our value for the resonance strength amounts to $(\omega\gamma)_{p\gamma}(E_R = 519\,\text{keV}) = (1.2 \pm 0.3) \times 10^{-2}\,\text{eV}$. The previously measured results are $(\omega\gamma)^{\text{Rolfs}}_{p\gamma} = (2.1 \pm 0.4) \times 10^{-2}\,\text{eV}$ [12] and $(\omega\gamma)^{\text{Sens}}_{p\gamma} = (7 \pm 2) \times 10^{-3}\,\text{eV}$ [13]. The former result was normalized to an erroneous value of the $E_R = 632\,\text{keV}$ resonance strength in the $^{27}Al(p,\gamma)^{28}Si$ reaction. Renormalization using the correct result (see Table I in Ref. [14]) gives $(\omega\gamma)^{\text{Rolfs}}_{p\gamma} = (1.3 \pm 0.3) \times 10^{-2}\,\text{eV}$, in agreement with the present value. Note, that the erroneous value for $(2J + 1)\Gamma_p\Gamma_\gamma/\Gamma$ is also listed in Table 18.31 of Ref. [3].

Figure 4 compares on- and off-resonance spectra measured in the $^{17}O(p,\gamma)^{18}F$ reaction at $E_p = 200$ (upper spectrum) and 228 keV (lower spectrum), respectively, i.e., in the energy region of the previously unmeasured $E_R \approx 190$ keV resonance. The spectrum measured at $E_p = 200\,\text{keV}$ clearly shows the full-energy and single-escape peaks for the primary $R \rightarrow 937$ keV and $R \rightarrow 1081$ keV transitions. The corresponding secondary transitions 937 keV$\rightarrow$0 and 1081 keV$\rightarrow$0 are also observed in the same spectrum (but are not shown in Fig. 4). Neither primary nor secondary transitions are observed in the off-resonance spectrum measured at $E_p = 228\,\text{keV}$. The excitation function of the primary $R \rightarrow 1081$ keV transition at bombarding energies around $\approx$200 keV is shown in Fig. 5. No yield is observed below and above the excitation function

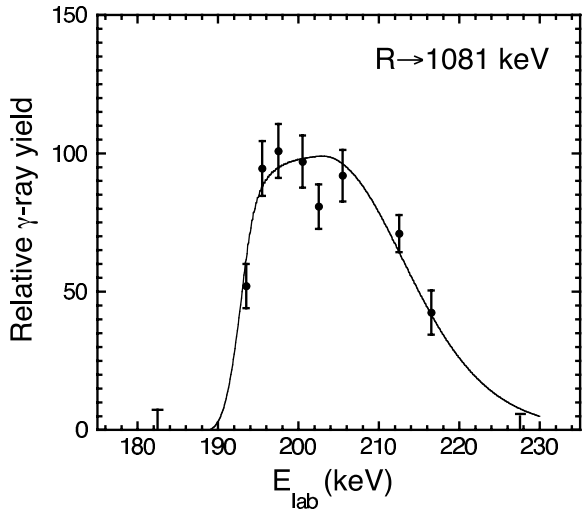

FIG. 5. Excitation function of the primary $R \rightarrow 1081$ keV transition for the newly discovered $E_R = 193$ keV resonance in $^{17}O(p,\gamma)^{18}F$. The solid line represents a numerical simulation showing the expected thick-target yield when the beam energy resolution and energy straggling in the target are taken into account.

(i.e., off-resonance), while the width of the measured yield curve agrees, after correction for stopping powers, with the one displayed in Fig. 3. We would like to emphasize that the data shown in Fig. 5 were obtained by using a different ^{17}O target compared to the results presented in our preliminary study (Fig. 2 in Ref. [2]). Furthermore, the data shown here represent a significant improvement in statistical accuracy.

From the measured yield curve, we obtain a resonance energy of $E_{R,1} = 193.3 \pm 1.5$ keV. The energy of the new resonance may also be calculated from the γ-ray energies of the primary transitions. For the excitation energy, we obtain values of $E_x = 5788.1 \pm 1.5$ and $E_x = 5789.6 \pm 1.4$ keV by using the measured energies of the $R \rightarrow 937$ keV and $R \rightarrow 1081$ keV transitions, respectively. These values are corrected for the nuclear recoil energy and for full Doppler shifts. The latter assumption is supported by the very short mean lifetime of this state [15]. The weighted average amounts to $E_x = 5788.9 \pm 1.0$ keV. From this value we calculate, by using the reaction Q value (see earlier), a resonance energy of $E_{R,2} = 193.2 \pm 1.2$ keV. We adopt the weighted mean of $E_R = 193.2 \pm 0.9$ keV. The resonance strength is calculated from the measured γ-ray intensities on the plateau of the thick-target yield curve according to Eqs. (2) and (3). The result is $(\omega\gamma)_{p\gamma}(E_R = 193\,\text{keV}) = (1.2 \pm 0.2) \times 10^{-6}$ eV, in excellent agreement with our preliminary value [2]. The error is mainly determined by uncertainties in γ-ray intensities, detection efficiencies, coincident summing corrections, and stopping powers. Angular correlation effects have been estimated by using the formalism presented in Ref. [16]. For pure transitions, the theoretical angular correlation functions are given by

$$W^{j_s=2}_{R\rightarrow 937}(E1) = 1 + 0.1 P_2(\cos\theta), \quad (4)$$

$$W^{j_s=3}_{R\rightarrow 937}(E1) = 1 - 0.0285 P_2(\cos\theta), \quad (5)$$

$$W^{j_s=2}_{R\rightarrow 1081}(E2) = 1 - 0.5 P_2(\cos\theta), \quad (6)$$

$$W^{j_s=3}_{R\rightarrow 1081}(E2) = 1 + 0.1428 P_2(\cos\theta), \quad (7)$$

with $j_s = 2$ or 3 denoting the channel spin. The channel spin mixing ratios for the primary transitions are not known. Nevertheless, we can estimate angular correlation effects by considering the pure transitions as extreme cases. The solid angle attenuation factor (Sec. II) at the energies of the primary transitions is about $Q_2 \approx 0.62$. Hence, the magnitude of the experimental angular correlation, $W_{\text{exp}} = 1 + a_2 Q_2 P_2(\cos\theta)$, for the $R \rightarrow 937$ keV transition becomes negligible compared to the error of $(\omega\gamma)_{p\gamma}$. The situation is not so clear for the $R \rightarrow 1081$ keV transition, which exhibits a large a_2 coefficient for the channel spin $j_s = 2$. In this case, we used the measured intensity of the corresponding secondary 1081 keV $\rightarrow$ 0 transition, which is isotropic (since $J_{1081} = 0$). Remaining angular correlation effects contribute less than 2% to the total error in the resonance strength and have been neglected. Our value of the resonance strength lies a factor of $\approx$330 below the upper limit reported by Ref. [15].

As a final experimental test, we measured the resonance strength of the well-known $E_R = 151$ keV resonance in ^{18}O$(p,\gamma)^{19}$F. We obtain a value of $(\omega\gamma)_{p\gamma}(E_R = 151\,\text{keV}) = (9.3 \pm 1.0) \times 10^{-4}$ eV, in agreement with the previously reported results of $(\omega\gamma)_{p\gamma}(E_R = 151\,\text{keV}) = (1.0 \pm 0.1) \times 10^{-3}$ eV [17] and $(9.2 \pm 0.6) \times 10^{-4}$ eV [18]. All of our measured energies and resonance strengths are summarized in Table I together with values reported in the literature.

IV. REACTION RATES

The total thermonuclear rate for the ^{17}O$(p,\gamma)^{18}$F reaction in units of cm^3 s^{-1} mole^{-1} is given by the expression [19]

$$N_A\langle\sigma v\rangle = 3.7318 \times 10^{10} \mu^{-1/2} T_9^{-3/2} \times \int_0^\infty \sigma(E) E e^{-11.605E/T_9} dE, \quad (8)$$

TABLE I. Summary of measured resonance energies and strengths in the (p,γ) reactions on ^{17}O and ^{18}O.

Reaction	E_R[a] (keV)	$(\omega\gamma)^{\text{present,b}}_{p\gamma}$ (eV)	$(\omega\gamma)^{\text{previous}}_{p\gamma}$ (eV)
^{17}O$(p,\gamma)^{18}$F	518.9 ± 1.0	$(1.2 \pm 0.3) \times 10^{-2}$	$(2.1 \pm 0.4) \times 10^{-2}$,[c]
			$(7 \pm 2) \times 10^{-3}$,[d]
^{17}O$(p,\gamma)^{18}$F	193.2 ± 0.9[e]	$(1.2 \pm 0.2) \times 10^{-6}$	$\leqslant 4 \times 10^{-4}$,[f]
^{18}O$(p,\gamma)^{19}$F	150.82 ± 0.09[g]	$(9.3 \pm 1.0) \times 10^{-4}$	$(9.2 \pm 0.6) \times 10^{-4}$,[h]
			$(1.0 \pm 0.1) \times 10^{-3}$,[i]

[a] From present work unless noted otherwise.
[b] From measured thick-target yield.
[c] Based on erroneous normalization (Sec. III); properly renormalized value is $\omega\gamma = (1.3 \pm 0.3) \times 10^{-2}$ eV.
[d] Based on unpublished stopping power values.
[e] Weighted average of directly measured resonance energy and value deduced from measured γ-ray energies of primary transitions (see text).
[f] From Ref. [15].
[g] Calibration value; from Ref. [5].
[h] From Ref. [17].
[i] From Ref. [18].

with E the center of mass energy in MeV, μ the reduced mass, and T_9 the temperature in GK. The total cross section σ (in barns) is determined by resonant and nonresonant contributions to the nuclear reaction mechanism. The contribution of isolated and narrow resonances to the total reaction rate is given by [19]

$$N_A\langle\sigma v\rangle_r = 1.540\times10^{11}(\mu T_9)^{-3/2}\sum_i(\omega\gamma)_i e^{-11.605E_i/T_9}, \tag{9}$$

with the center of mass energies E_i and strengths $(\omega\gamma)_i$ of the resonances in MeV. Nonresonant cross sections vary smoothly with (center of mass) bombarding energy E and are usually converted into the astrophysical S factor, defined by

$$S(E) = \sigma(E)Ee^{2\pi\eta}, \tag{10}$$

with η denoting the Sommerfeld parameter. If the S factor can be approximated by a polynomial

$$S(E) = S(0) + ES'(0) + \tfrac{1}{2}E^2S''(0), \tag{11}$$

then the nonresonant reaction rates are obtained by using the relations [19]

$$N_A\langle\sigma v\rangle_{\rm nr} = 4.339\times10^8\tau^2\frac{1}{\mu Z_pZ_t}e^{-\tau}S_{\rm eff}, \tag{12}$$

$$S_{\rm eff} = S(0)\left[1+\frac{5}{12\tau}+\frac{S'(0)}{S(0)}\left(E_0+\frac{35}{36}kT\right)+\frac{1}{2}\frac{S''(0)}{S(0)}\left(E_0^2+\frac{89}{36}E_0kT\right)\right], \tag{13}$$

with Z_p and Z_t the charges of the projectile and target, respectively, $E_0 = 0.122(Z_p^2Z_t^2\mu T_9^2)^{1/3}$ the location of the Gamow peak in MeV, k the Boltzmann constant, $S_{\rm eff}$ the effective S factor in (MeV b), and $\tau = 4.249(Z_p^2Z_t^2\mu/T_9)^{1/3}$. The various resonant and nonresonant contributions to the total rate are discussed in more detail below.

A. Narrow resonances

All experimentally observed $^{17}O(p,\gamma)^{18}F$ resonances in the energy range $E_R = 70$–1346 keV have been considered for the sum in Eq. (9). Resonance energies were calculated from the excitation energies compiled in Ref. [3] by using $Q_{p\gamma} = 5606.5\pm0.5$ keV [4], except for the new $E_R = 193$ keV resonance for which the value listed in Table I is adopted. Measured strengths of resonances at $E_R \geqslant 531$ keV are obtained from Refs. [12,13]. We renormalized the $(\omega\gamma)_{p\gamma}$ values of Ref. [12] by using the correct resonance strength for $E_R =$ 632 keV in $^{27}Al(p,\gamma)^{28}Si$ (see Sec. II). The $(\omega\gamma)_{p\gamma}$ values presented in Ref. [13] are adopted without changes since they were normalized relative to the (correct) resonance strength for $E_R = 655$ keV in $^{27}Al(p,\gamma)^{28}Si$. Weighted averages of both sets of $(\omega\gamma)_{p\gamma}$ values are adopted in the present work. For the resonances at $E_R = 193$ and 519 keV, our measured $(\omega\gamma)_{p\gamma}$ values are used (Table I).

The case of the $E_R = 70$ keV resonance, corresponding to the ^{18}F level at $E_x = 5673$ keV ($J^\pi = 1^-$), deserves special attention. For this level, three important quantities are known. (i) The resonance strength in the $^{17}O(p,\alpha)^{14}N$ reaction has been measured by Ref. [20]; we use a value of $(\omega\gamma)_{p\alpha} = (4.7\pm0.8)\times10^{-9}$ eV, which is slightly different from the one reported in Ref. [20] because we take into account the results from an independent reanalysis [21] of the original data. (ii) The resonance strength in the $^{14}N(\alpha,\gamma)^{18}F$ reaction has been measured; the average value of the results reported by Refs. [22–25] amounts to $(\omega\gamma)_{\alpha\gamma} = 0.44\pm0.02$ eV. (iii) The α partial width was deduced from an R-matrix analysis of $^{14}N(\alpha,\alpha)$ scattering data [26], with the result of $\Gamma_\alpha = 130\pm5$ eV. From these three quantities we can calculate the strength of the (p,γ) resonance. The result is $(\omega\gamma)_{p\gamma} = (1.6\pm0.3)\times10^{-11}$ eV. A significantly larger value, $(\omega\gamma)_{p\gamma} = 5.9^{+1.9}_{-1.1}\times10^{-11}$ eV, was used by the NACRE Collaboration [1]. Their result is based on the value of $\Gamma_\gamma = 1.4\pm0.3$ eV [26], which was calculated from the measured Γ_α value [26] and a "strength of $(\omega\gamma)_{\alpha\gamma} = 1.37\pm0.19$ eV" from Ref. [24]. However, the latter value represents the quantity $(2J+1)\Gamma_\alpha\Gamma_\gamma/\Gamma$ instead of $(\omega\gamma)_{\alpha\gamma}$ [Eq. (1)]. Since the ^{14}N target spin was disregarded in the previous analysis, both the value of Γ_γ quoted above and the $(\omega\gamma)_{p\gamma}$ value adopted by Ref. [1] are erroneous. As will be seen below, the proper inclusion of the spin factor decreases the total reaction rates by a factor of $\approx$3 at stellar temperatures of $T = 0.03-0.09$ GK.

Random errors for E_R and $\omega\gamma$ are explicitly taken into account in the calculation of the narrow resonance reaction rates. Statistical uncertainties in $N_A\langle\sigma v\rangle_r$ are estimated following the formalism presented in Ref. [27], to which the reader is referred for details.

B. Direct capture

The total direct capture (DC) cross section is given by an incoherent sum over (i) all orbital angular momenta of the initial scattering state (ℓ_i) and the final state (ℓ_f) and (ii) all final states j

$$\sigma^{\rm DC}_{\rm total} = \sum_j\sum_{\ell_i\ell_f}C^2S_j(\ell_f)\sigma^{\rm DC}_{{\rm calc},j}(\ell_i,\ell_f), \tag{14}$$

with $S(\ell_f)$ and C denoting the single-particle spectroscopic factor and the isospin Clebsch-Gordan coefficient ($C^2 = 1/2$ for $^{17}O + p \rightarrow {}^{18}F$), respectively. For the spectroscopic factors, we adopted the average of the experimental values reported by Refs. [28,29]. The theoretical direct capture cross section $\sigma^{\rm DC}_{\rm calc}$ is calculated by using a single-particle potential model. The cross section for a transition to a specific final state is determined by the overlap of the scattering wave function in the entrance channel, the bound state wave function in the exit channel, and the electromagnetic multipole transition operator. The radial wave function for the final bound state is generated by using a Woods-Saxon potential with radius parameter $r_0 = 1.25$ fm and diffuseness $a = 0.65$ fm (i.e., the *same* values that were used in the transfer studies of Refs. [28,29]). The well depth is chosen to reproduce the binding energy of the final state. A hard-sphere potential of radius $R = 1.25(17)^{1/3} = 3.2$ fm is used for calculating the scattering state radial wave function. Only $E1$ γ-ray transitions are taken into account since calculations performed for other multipoles

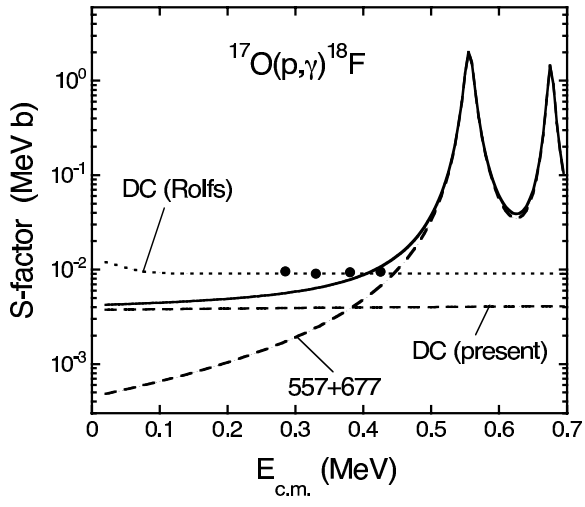

FIG. 6. Previous [12] and present total direct capture (DC) S-factor extrapolations are displayed as dotted and dashed lines, respectively. The incoherent sum of the S factors from the broad resonances at $E_R = 589$ keV ($E_R^{\text{c.m.}} = 557$ keV, $J^\pi = 3^+$) and $E_R = 716$ keV ($E_R^{\text{c.m.}} = 677$ keV, $J^\pi = 2^+$) is also shown as a dashed line. The solid line represents the sum of the present direct capture S-factor and resonance tail contributions. The data points at $E \approx 0.3-0.4$ MeV are from Fig. 17 of Ref. [12].

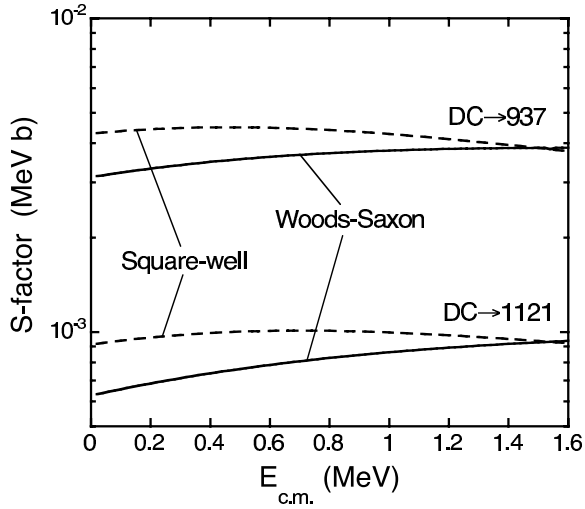

FIG. 7. Calculated $^{17}\text{O} + p$ direct capture S factors for the transitions DC $\rightarrow$ 937 keV and DC $\rightarrow$ 1121 keV. The dashed and solid lines are obtained by using a square-well and a Woods-Saxon potential, respectively, for calculating the bound state radial wave function. For each transition, the dashed and solid lines are normalized to the same cross section at $E_p \approx 1.6$ MeV.

indicate that their contributions are negligible. In total, direct capture transitions into 21 final bound states in ^{18}F are taken into account. For energies below $E = 1$ MeV, we find for the total direct capture S factor (with E in MeV and $S(E)$ in MeV b),

$$S(E) = 0.00374 + 0.000676E - 0.000249E^2. \qquad (15)$$

This result is displayed in Fig. 6 as a dashed curve. We assumed random errors of 50% in the experimental C^2S values. This uncertainty is explicitly taken into account for the calculation of the total reaction rate errors (see Ref. [27] for details).

The method outlined above for estimating the direct capture contribution has been applied to numerous calculations of thermonuclear reaction rates and is well established (see, for example, Ref. [14]). Furthermore, a recent systematic study [30] has shed some light on the role of scattering and bound state potential parameters for calculating $\sigma_{\text{calc}}^{\text{DC}}$. It is important to emphasize that previous estimates [1,29,31] of direct capture S factors for $^{17}\text{O} + p$ employed a different method. These authors adopted the S factor of Ref. [12] that was obtained by extrapolating the total cross section measured at higher energies ($E_p \approx 1.6$ MeV according to Table II of Ref. [12]) down to stellar energies "via the direct-capture model." Their result exceeds the present estimate by a factor of $\approx$2.5 (see dotted line in Fig. 6). We have reservations about their procedure for two main reasons described next.

First, the direct capture model calculations in Ref. [12] are performed by using a square-well potential with radius parameter of $r_0 = 1.36$ fm for generating the bound state radial wave function. It has been shown previously [30,32] that direct capture cross sections obtained from square-well potentials differ by factors of up to $\approx$3 from those generated by using more realistic Woods-Saxon potentials. The use of square-well potentials does not only change the magnitude of the cross section, but changes the *energy dependence* of $\sigma_{\text{calc}}^{DC}$ as well. This is demonstrated in Fig. 7, showing direct capture S factors for two sample transitions (DC $\rightarrow$ 937 keV and DC $\rightarrow$ 1121 keV, representing $\ell_i = 1 \rightarrow \ell_f = 0$ and $\ell_i = 1 \rightarrow \ell_f = 2$ transitions, respectively). The dashed and solid lines are obtained by using a square-well and a Woods-Saxon potential, respectively, for calculating the bound state radial wave function. For the former potential, we employ the same parameters that were used in the original study of Ref. [12]. For each transition, the dashed and solid lines are normalized to the same cross section at $E_p \approx$ 1.6 MeV, i.e., the bombarding energy at which the experimental direct capture cross sections for the different transitions have been measured (see Table II in Ref. [12]). It is obvious that the choice of bound state potential has a large influence on the extrapolation of the S factor to low energies. We find that the S factors at $E \approx 0$ for the two transitions shown are smaller by 40 and 45%, respectively, when a realistic Woods-Saxon potential is used. Similar results are expected for other direct capture transitions in $^{17}\text{O} + p$. It is also interesting to note that we find no evidence of the upturn of the S factor at low energies that was reported by Ref. [12] (see our Fig. 6 or Fig. 17 of Ref. [12]), by using either a square-well or a Woods-Saxon potential.

Second, in view of the arguments presented above, it is surprising that the extrapolated S factor of Ref. [12] agrees with the four data points shown in Fig. 17 of Ref. [12] (also displayed in our Fig. 6). These data points presumably represent measured direct capture cross sections. On the contrary, we have reasons to assume that these "direct capture cross section data points" are influenced by the tails of higher

lying broad resonances. This is demonstrated in Fig. 6 showing the incoherent sum of the S factors from the broad resonances at $E_R = 589$ keV ($J^\pi = 3^+$, $\Gamma = 14$ keV) and $E_R = 716$ keV ($J^\pi = 2^+$, $\Gamma = 10$ keV) as a dashed line, and the sum of present resonant and direct capture S factors as the solid line. The calculation of broad-resonance tails will be described in Sec. IV C. Clearly, the two higher lying data points ($E \approx 0.4$ MeV) are entirely explained by the incoherent sum of the present direct capture S factor and the broad-resonance tails. In fact, the disturbing presence of these two broad resonances is mentioned by Ref. [12] as a reason for studying the $^{17}O + p$ direct capture transitions in detail only at energies of $E_p \geqslant 900$ keV. Therefore, it is not clear at all how (and if) the four "direct capture cross section data points" at $E \approx 0.3$–0.4 MeV shown in Fig. 17 of Ref. [12] have been corrected for resonance tail contributions. It should be emphasized that interference effects between direct capture and the two broad resonances mentioned above are expected to be negligible for the total cross section since these processes proceed via different orbital angular momenta ($\ell_i = 1$ and $\ell_R = 0$, respectively).

These considerations are important since it will be shown below that the direct capture process dominates the total reaction rates in the temperature regions of $T \leqslant 0.03$ and $T = 0.09$–0.4 GK.

C. Broad resonances

The reaction rate contribution of high-energy tails from subthreshold resonances is estimated by describing the S factor according to the Breit-Wigner formula with energy-dependent partial widths and the Thomas approximation [33] as

$$S_{\rm SR}(E) = E e^{2\pi\eta} \frac{\pi}{k^2} \frac{\Gamma_p(E)\Gamma_\gamma(E)}{(E - E_r)^2 + \frac{1}{4}[\Gamma(E)]^2}, \qquad (16)$$

with k the wave number and E_r the center-of-mass resonance energy. The proton and γ-ray partial widths are given by

$$\Gamma_p(E) = 2\frac{\hbar^2}{\mu R^2} P(E) C^2 S \theta_{\rm sp}^2, \qquad (17)$$

$$\Gamma_\gamma(E) = \Gamma_\gamma(E_r) B_\gamma \left(\frac{E + Q_{p\gamma} - E_f}{E_r + Q_{p\gamma} - E_f} \right)^{2L+1}, \qquad (18)$$

with $R = 1.25\,(17^{1/3} + 1) = 4.5$ fm the channel radius, $P(E)$ the penetration factor, $\theta_{\rm sp}^2$ the (observed) dimensionless single-particle reduced width [34], B_γ the primary γ-ray branching ratio to the final state at E_f, and L the multipolarity of the γ-ray transition under consideration. Values of C^2S are adopted from Refs. [28,29] while those for $\Gamma_\gamma(E_r)$ are calculated either from measured lifetimes τ_m [3] or from measured strengths $(\omega\gamma)_{\alpha\gamma}$ [22–25] and α-particle widths Γ_α [26]. The largest S-factor contributions arise from the levels at $E_x = 3839$ ($\ell_p = 0$), 5603 ($\ell_p = 2$), and 5605 ($\ell_p = 1$) keV. However, their total contribution to the reaction rates is found to be negligible compared to those from narrow resonances and direct capture at all temperatures.

The narrow-resonance reaction rate formalism [Eq. (9)] neglects the energy dependence of the Maxwell-Boltzmann distribution and, therefore, takes only the reaction rate contribution at the resonance energy E_r into account. Hence, it is important to estimate the contributions from low-energy tails of resonances, especially those with measured total widths. The S factor can be expressed in terms of resonance strengths and total widths as

$$S_{\rm BR}(E) = \frac{\pi\hbar^2}{2\mu} e^{2\pi\eta} \frac{P(E)}{P(E_r)} \left(\frac{E + Q - E_f}{E_r - Q - E_f} \right)^{2L+1} \times \frac{(\omega\gamma)_{p\gamma}\Gamma(E_r)}{(E_r - E)^2 + \frac{1}{4}[\Gamma(E)]^2}. \qquad (19)$$

Experimental values of $(\omega\gamma)_{p\gamma}$ and Γ for resonances at $E_R = 519$–1239 keV are adopted from Refs. [12,13] (Sec. IV A) and Ref. [35], respectively. At energies below $E = 0.23$ MeV, we obtain for the total S factor from tails of broad resonances [with E in MeV and $S(E)$ in MeV b]

$$S(E) = 0.000464 + 0.000917E + 0.00963E^2. \qquad (20)$$

The largest contributions arise from the resonances at $E_R = 557$ and 677 keV (Sec. IV B and Fig. 6).

We also integrated the reaction rate contributions of the two lowest-lying resonances at $E_R = 70$ and 193 keV numerically [according to Eq. (8)] in order to investigate the influence of their low-energy tails. We find indeed that these tails provide reaction rate contributions at low temperatures, $T < 0.04$ GK, far in excess of those calculated according to the narrow-resonance formalism [Eq. (9)]. Nevertheless, the tail contributions of the $E_R = 70$ and 193 keV resonances are negligible compared to the direct capture process at all temperatures.

D. Total reaction rates

The total reaction rates, given by an incoherent sum of the individual contributions discussed above, are listed in Table II for temperatures of $T = 0.01 - 1.5$ GK. Upper and lower limits of the total rates are also given. These represent *statistical* uncertainties corresponding to a 65–68% confidence belt [27]. The total reaction rates are also displayed in Fig. 8. The significant improvement in accuracy compared to Fig. 1 is evident. For example, at $T = 0.2$ GK the uncertainty in the $^{17}O(p,\gamma)^{18}F$ reaction rates is reduced from orders of magnitude to ≈30%. Note that at temperatures below $T = 0.03$ GK, where the direct capture process dominates (see below), the errors in the present rates (≈50%) are in fact larger than those presented previously (≈20% according to Ref. [1]). In view of the discussion presented in Sec. IV B, we regard a value of only 20% for the direct capture reaction rate error as being unrealistic.

Individual rate contributions are displayed in Fig. 9 as fractions relative to the total recommended rates listed in Table II. Below T = 0.03 GK, the direct capture process dominates the total rates, with the contribution from low-energy tails of broad resonances amounting to about 10%. At $T = 0.03$–0.09 GK, the $E_R = 70$ keV resonance contributes up to 80%

TABLE II. Total thermonuclear reaction rates for $^{17}O(p,\gamma)^{18}F$.

T (GK)	Lower limit	Recommended	Upper limit
0.01	1.97×10^{-25}	3.03×10^{-25}	4.76×10^{-25}
0.011	2.10×10^{-24}	3.22×10^{-24}	5.06×10^{-24}
0.012	1.70×10^{-23}	2.60×10^{-23}	4.09×10^{-23}
0.013	1.10×10^{-22}	1.69×10^{-22}	2.65×10^{-22}
0.014	5.94×10^{-22}	9.10×10^{-22}	1.43×10^{-21}
0.015	2.75×10^{-21}	4.21×10^{-21}	6.61×10^{-21}
0.016	1.11×10^{-20}	1.71×10^{-20}	2.68×10^{-20}
0.018	1.33×10^{-19}	2.03×10^{-19}	3.19×10^{-19}
0.02	1.14×10^{-18}	1.73×10^{-18}	2.70×10^{-18}
0.025	1.10×10^{-16}	1.55×10^{-16}	2.22×10^{-16}
0.03	5.68×10^{-15}	7.32×10^{-15}	9.49×10^{-15}
0.04	1.57×10^{-12}	1.96×10^{-12}	2.46×10^{-12}
0.05	5.12×10^{-11}	6.31×10^{-11}	7.78×10^{-11}
0.06	5.33×10^{-10}	6.49×10^{-10}	7.91×10^{-10}
0.07	2.93×10^{-9}	3.56×10^{-9}	4.33×10^{-9}
0.08	1.11×10^{-8}	1.37×10^{-8}	1.69×10^{-8}
0.09	3.37×10^{-8}	4.29×10^{-8}	5.50×10^{-8}
0.1	9.13×10^{-8}	1.20×10^{-7}	1.60×10^{-7}
0.11	2.34×10^{-7}	3.16×10^{-7}	4.31×10^{-7}
0.12	5.77×10^{-7}	7.84×10^{-7}	1.08×10^{-6}
0.13	1.36×10^{-6}	1.84×10^{-6}	2.52×10^{-6}
0.14	3.03×10^{-6}	4.07×10^{-6}	5.52×10^{-6}
0.15	6.36×10^{-6}	8.45×10^{-6}	1.13×10^{-5}
0.16	1.25×10^{-5}	1.65×10^{-5}	2.18×10^{-5}
0.18	4.06×10^{-5}	5.27×10^{-5}	6.90×10^{-5}
0.2	1.08×10^{-4}	1.40×10^{-4}	1.82×10^{-4}
0.25	6.06×10^{-4}	8.16×10^{-4}	1.10×10^{-3}
0.3	2.47×10^{-3}	3.35×10^{-3}	4.53×10^{-3}
0.35	1.02×10^{-2}	1.31×10^{-2}	1.67×10^{-2}
0.4	4.63×10^{-2}	5.46×10^{-2}	6.45×10^{-2}
0.45	1.84×10^{-1}	2.09×10^{-1}	2.37×10^{-1}
0.5	5.95×10^{-1}	6.67×10^{-1}	7.48×10^{-1}
0.6	3.62×10^{0}	4.04×10^{0}	4.51×10^{0}
0.7	1.32×10^{1}	1.48×10^{1}	1.65×10^{1}
0.8	3.48×10^{1}	3.87×10^{1}	4.30×10^{1}
0.9	7.29×10^{1}	8.10×10^{1}	9.00×10^{1}
1.0	1.31×10^{2}	1.45×10^{2}	1.61×10^{2}
1.25	3.62×10^{2}	4.00×10^{2}	4.42×10^{2}
1.5	6.90×10^{2}	7.60×10^{2}	8.37×10^{2}

to the total rate. Between $T = 0.09$ and 0.35 GK, the direct capture process again provides the largest contribution to the total rates, while the $E_R = 193$ keV resonance contributes at most a fraction of ≈40% (around $T = 0.2$ GK). This result is surprising in the sense that for most other reactions, the total rates are dominated by resonances if they are located in the Gamow window. However, for the $^{17}O(p,\gamma)^{18}F$ reaction, the $E_R = 193$ keV resonance is relatively weak and it is the only resonance located between $E_R = 70$ and 519 keV. Above $T = 0.35$ GK, higher lying resonances with $E_R \geqslant 519$ keV dominate the total reaction rates.

The ratio of present and previous [1] total recommended reaction rates for $^{17}O(p,\gamma)^{18}F$ is displayed in Fig. 10. Above $T = 0.5$ GK, both results are in agreement. At $T = 0.09-0.5$ GK, our rates are smaller than the previous values by up to a factor of 10 because of the much reduced contribution from

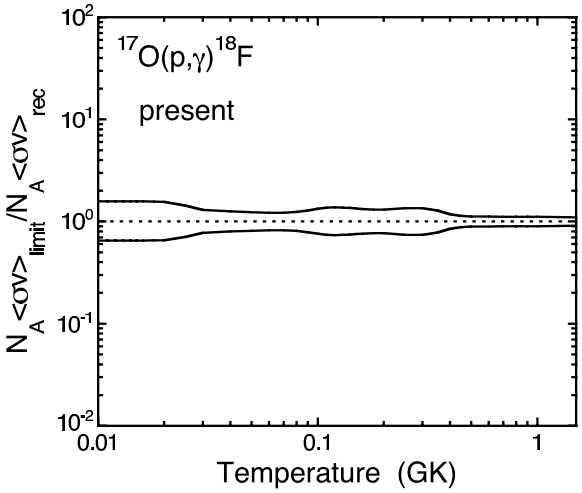

FIG. 8. Same as Fig. 1, but with $^{17}O(p,\gamma)^{18}F$ reaction rates from present work. Comparison to Fig. 1 reveals the dramatic reduction in reaction rate uncertainties due to the observation of the $E_R = 193$ keV resonance.

the $E_R = 193$ keV resonance (see also Fig. 9) which has been measured in the present work. Between $T = 0.03$ and 0.09 GK, the total rates are decreased by a factor of ≈3 because the spin factor was erroneously disregarded in the previous analysis [1] (see Sec. IV A). Below $T = 0.03$ GK, our total rates are smaller than the previous results by a factor of ≈2.5 because we assumed a reduced direct capture contribution (see Sec. IV B).

We have discussed so far only reaction rate uncertainties caused by *statistical* errors in experimental values for resonance energies E_R, resonance strengths $\omega\gamma$, and spectroscopic factors C^2S. We will briefly comment on potential *systematic* errors in $^{17}O(p,\gamma)^{18}F$ reaction rates. Recall that the strength

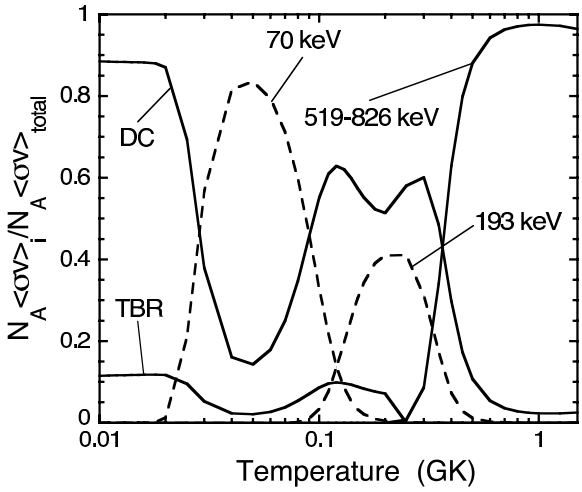

FIG. 9. Ratios of individual reaction rate contributions and the total recommended rate that is listed in Table II. The two dashed lines show the components arising from the two lowest-lying resonances. Contributions from direct capture and the low-energy tails of broad resonances are denoted by DC and TBR, respectively. All resonance energies correspond to laboratory values.

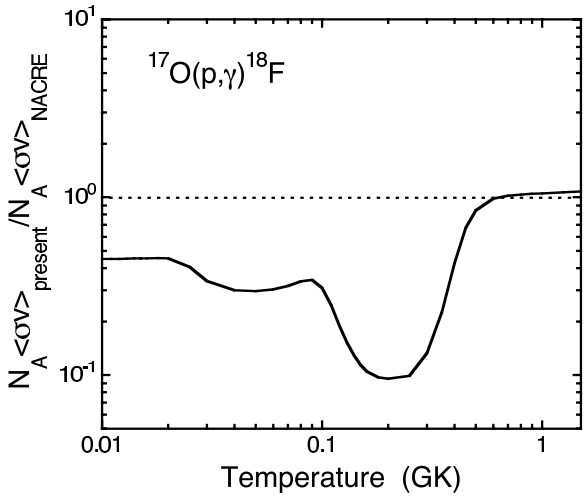

FIG. 10. Ratio of present and previous [1] total recommended reaction rates for $^{17}O(p,\gamma)^{18}F$.

$(\omega\gamma)_{p\gamma}$ of the $E_R = 70$ keV resonance was not measured directly but was inferred from measured values of $(\omega\gamma)_{p\alpha}$, $(\omega\gamma)_{\alpha\gamma}$, and Γ_α (Sec. IV A). Although a direct measurement of this resonance in the (p,γ) channels seems at present beyond experimental capabilities, we nevertheless regard the derived resonance strength as sufficiently reliable. The situation is not as clear for the direct capture contribution. It must again be emphasized that the direct capture S factor was measured only at higher energies and had to be extrapolated to the low-energy range for calculating the reaction rates. Our direct capture S factor deviates significantly from the results of an earlier analysis [12] as discussed in Sec. IV B. Although quite a challenging task, reanalyzing existing data for $^{17}O(p,\gamma)$, (p,α), and (p,p) and for $^{14}N(\alpha,\gamma)$ and (α,α) by using an R-matrix formalism, may prove worthwhile. Such an analysis is beyond the scope of the present work but may provide an estimate of interference effects between various cross-section contributions.

V. SUMMARY AND CONCLUSIONS

We reported on a measurement of the $^{17}O(p,\gamma)^{18}F$ reaction in the energy range of $E_p = 180$–540 keV. A previously undiscovered resonance is observed at $E_R = 193.2 \pm 0.9$ keV. The resonance strength amounts to $(\omega\gamma)_{p\gamma} = (1.2 \pm 0.2) \times 10^{-6}$ eV. With this value, previous uncertainties in the $^{17}O(p,\gamma)^{18}F$ reaction rates are reduced by orders of magnitude at temperatures of $T = 0.1-0.5$ GK (i.e., the range of nova peak temperatures). At these temperatures, our total rates are smaller by up to a factor of 10 compared to results reported by the NACRE Collaboration. The present reaction rates differ also significantly from the previous results (by factors of $\approx 2-3$) at the lower temperatures of interest to the study of red giants, AGB stars, and massive stars. These differences are mainly caused by unreliable previous assumptions for the $E_R = 70$ keV resonance strength and the extrapolated direct capture S factor at low energies. The present work establishes the $^{17}O(p,\gamma)^{18}F$ reaction rates over a temperature range of $T = 0.01-1.5$ GK with statistical uncertainties of 10–50%. Several effects that may give rise to systematic uncertainties in the reaction rates have also been discussed.

ACKNOWLEDGMENT

This work was supported in part by the U.S. Department of Energy under Contract No. DE-FG02-97ER41041.

[1] C. Angulo *et al.*, Nucl. Phys. **A656**, 3 (1999).
[2] C. Fox, C. Iliadis, A. E. Champagne, A. Coc, J. José, R. Longland, J. Newton, J. Pollanen, and R. Runkle, Phys. Rev. Lett. **93**, 081102 (2004).
[3] D. R. Tilley, H. R. Weller, C. M. Cheves, and R. M. Chasteler, Nucl. Phys. **A595**, 1 (1995).
[4] G. Audi, A. H. Wapstra, and C. Thibault, Nucl. Phys. **A729**, 337 (2003).
[5] H. W. Becker *et al.*, Z. Phys. A **351**, 453 (1995).
[6] D. Phillips and J. P. S. Pringle, Nucl. Instrum. Methods **135**, 389 (1976).
[7] D. A. Vermilyea, Acta Metall. **1**, 282 (1953).
[8] K. Debertin and R. G. Helmer, *Gamma- and X-ray Spectrometry with Semiconductor Detectors* (North-Holland, Amsterdam, 1988).
[9] T. Semkow, G. Mehmood, P. Parekh, and M. Virgil, Nucl. Instrum. Methods A **290**, 437 (1990).
[10] H. E. Gove, in *Nuclear Reactions I*, edited by P. M. Endt and M. Demeur (North Holland, Amsterdam, 1959).
[11] J. F. Ziegler and J. P. Biersack, computer program SRIM, 2003.
[12] C. Rolfs, Nucl. Phys. **A217**, 29 (1973).
[13] J. C. Sens, A. Pape, and R. Armbruster, Nucl. Phys. **A199**, 241 (1973).
[14] C. Iliadis, J. D'Auria, S. Starrfield, W. J. Thompson, and M. Wiescher, Astrophys. J. Suppl. **134**, 151 (2001).
[15] C. Rolfs, I. Berka, and R. E. Azuma, Nucl. Phys. **A199**, 306 (1973).
[16] L. C. Biedenharn, in *Nuclear Spectroscopy*, edited by F. Ajzenberg-Selove (Academic Press, New York, 1960).
[17] M. Wiescher *et al.*, Nucl. Phys. **A349**, 165 (1980).
[18] R. B. Vogelaar, T. R. Wang, S. E. Kellogg, and R. W. Kavanagh, Phys. Rev. C **42**, 753 (1990).
[19] W. A. Fowler, G. R. Caughlan, and B. A. Zimmerman, Annu. Rev. Astron. Astrophys. **5**, 525 (1967).
[20] J. C. Blackmon, A. E. Champagne, M. A. Hofstee, M. S. Smith, R. G. Downing, and G. P. Lamaze, Phys. Rev. Lett. **74**, 2642 (1995).
[21] M. D. Hannam and W. J. Thompson, Nucl. Instrum. Methods A **431**, 239 (1999).
[22] P. D. Parker, Phys. Rev. **173**, 1021 (1968).
[23] C. Rolfs, A. M. Charlesworth, and R. E. Azuma, Nucl. Phys. **A199**, 257 (1973).

[24] I. Berka, K. P. Jackson, C. Rolfs, A. M. Charlesworth, and R. E. Azuma, Nucl. Phys. **A288**, 317 (1977).
[25] H. W. Becker, W. E. Kieser, C. Rolfs, H. P. Trautvetter, and M. Wiescher, Z. Phys. A **305**, 319 (1982).
[26] H.-B. Mak, G. T. Ewan, H. C. Evans, J. D. MacArthur, and W. McLatchie, Nucl. Phys. **A343**, 79 (1980).
[27] W. J. Thompson and C. Iliadis, Nucl. Phys. **A647**, 259 (1999).
[28] L. M. Polsky, C. H. Holbrow, and R. Middleton, Phys. Rev. **186**, 966 (1969).
[29] V. Landre, P. Aguer, G. Bogaert, A. Lefebvre, and J. P. Thibaud, Phys. Rev. C **40**, 1972 (1989).
[30] C. Iliadis and M. Wiescher, Phys. Rev. C **69**, 064305 (2004).
[31] C. Rolfs and W. S. Rodney, Nucl. Phys. **A250**, 295 (1975).
[32] D. C. Powell, C. Iliadis, A. E. Champagne, C. A. Grossmann, S. E. Hale, V. Y. Hansper, and L. K. McLean, Nucl. Phys. **A660**, 349 (1999).
[33] R. G. Thomas, Phys. Rev. **81**, 148 (1951).
[34] C. Iliadis, Nucl. Phys. **A618**, 166 (1997).
[35] W. E. Kieser, R. E. Azuma, and K. P. Jackson, Nucl. Phys. **A331**, 155 (1979).